Advance material modulation of nutritional and phytohormone status alleviates damage from soybean sudden death syndrome (SDS) and increases crop growth Chuanxin Ma^{1, 2}, Java Borgatta¹, Blake Geoffrey Hudson³, Ali Abbaspour Tamijani³, Roberto De La Torre-Roche², Nubia Zuverza-Mena², Yu Shen^{1,2}, Wade Elmer⁴, Baoshan Xing⁵, Sara Elizabeth Mason³, Robert John Hamers¹, Jason Christopher White^{2,*} ¹The Center for Sustainable Nanotechnology, Department of Chemistry, University of Wisconsin, Madison, Wisconsin 53706, USA; ²The Center for Sustainable Nanotechnology, Department of Analytical Chemistry, The Connecticut Agricultural Experiment Station, New Haven, Connecticut 06504, USA; ³The Center for Sustainable Nanotechnology, Department of Chemistry, University of Iowa, Iowa City, Iowa 52242, USA; ⁴The Center for Sustainable Nanotechnology, Department of Plant Pathology and Ecology, The Connecticut Agricultural Experiment Station, New Haven, Connecticut 06504, USA; ⁵Stockbridge School of Agriculture, University of Massachusetts, Amherst, Massachusetts 01003, USA *Corresponding author: Jason.White@ct.gov

Abstract Customized Cu₃(PO₄)₂ and CuO nanosheets (NS) and commercial CuO nanoparticles (NPs) were investigated for micronutrient delivery and suppression of soybean sudden death syndrome. An *ab initio* thermodynamics approach modeled how material morphology and matrix effects control nutrient release. Infection reduced biomass and photosynthesis by 70.3% and 60%, respectively; foliar application of nanoscale Cu reversed this damage. Disease-induced changes in antioxidant enzyme activity and fatty acid profile were also alleviated by Cu-amendment. The transcription of two dozen defense- and health-related genes correlate nanoscale Cu-enhanced innate disease response to reduced pathogenicity and increased growth. Cu-based NS exhibited greater disease suppression than CuO NPs due to greater leaf surface affinity and Cu dissolution as determined computationally and experimentally. The findings highlight the importance and tunability of nanomaterial properties such as morphology, composition, and dissolution. Early seedling foliar application of nanoscale Cu to modulate nutrition and enhance immunity offer great potential for sustainable agriculture.

Low use efficiency of fertilizers in agriculture confounds global food security, particularly given the 60-70% increase in food production needed by 2050. Nearly 70% of applied fertilizers are not used by crops, wasting energy and water, and causing environmental damage. Novel and sustainable food production strategies are sorely needed. Nano-enabled agrichemicals have attracted attention as surface-modified and customized nanomaterials (NMs) could release nutrients at controllable rates and activate plant defense systems to suppress disease. Given the role of micronutrients in plant growth and disease defense, mechanistic investigation into nanoscale micronutrient platforms is warranted.

Engineered nanoparticles (NPs) can enhance plant growth and suppress disease.^{3,4} Although micronutrients are not basipetally translocated to root tissues, ⁵ a split root experiment demonstrated phloem-based CuO NP transport.⁶ Nanoscale micronutrients such as CuO, Fe₂O₃, and ZnO increased nutrient uptake^{7, 8, 9, 10}, and alleviated root and leaf damage caused by the fungal pathogens.^{10, 11, 12} Importantly, disease suppression is through modulated plant nutrition and not toxicity against the pathogen. Notably, material properties (shape, composition, etc.) can be "tuned" to control activity. Borgatta et al. demonstrated that foliar exposure of watermelon to Cu₃(PO₄)₂ nanosheets (NS) at 10 mg/L suppressed *Fusarium* infection, whereas CuO NPs exerted similar impacts at 250-1000 mg/L.¹³ This increased NS response was correlated with more rapid upregulation of plant defense genes as a function of material properties.¹⁴

Fusarium virguliforme (FV) is a root fungal pathogen that causes sudden death syndrome (SDS) to soybean (*Glycine max*).^{15, 16} SDS is widespread in the United States and has resulted in \$3.06 billion in losses.¹⁷ FV resides in the soil, infects roots, and colonizes xylem and phloem elements. The export of toxins to the shoots, along with physically restricted water and nutrient transport, compromises photosynthesis, growth, and yield.¹⁸ Early symptoms include poor root development, foliar chlorosis/necrosis, and defoliation; however, symptoms often intensify at flowering, followed by rapid mortality.¹⁵ SDS Management has been difficult,

although crop rotation and improved soil drainage offer some benefit.¹⁹ Given the disease suppressive effect of nanoscale micronutrients^{10, 13-14}, investigation into this approach for SDS was pursued.

Micronutrient delivery and SDS suppression was investigated with two types of Cu-based nanosheets (NS), Cu₃(PO₄)₂ NS and CuO NS, and commercial CuO NPs. Soybean plants were grown in a greenhouse with or without FV infection that were foliar-amended with Cu-NMs. Endpoints included phenotype, biomass, photosynthesis, nutrient content, fatty acid profile, and the expression of defense-related genes. The materials were modeled with density functional theory and thermodynamics to determine how morphology and solution properties control dissolution. This study uses foliar Cu-based NMs to prevent crop damage from a root fungal pathogen and highlights nano-enabled modulation of plant nutrition as a novel and sustainable strategy for disease management.

Nanomaterial characterization and dissolution

Nanomaterial characterization data is in the supplementary information. $^{13-14}$ SEM shows that $Cu_3(PO_4)_2$ NS (exists as hydrated $Cu_3(PO_4)_2 \cdot 3H_2O$) and CuO NS possess sheet-like morphology (**Figure S1a and c**); commercial CuO NPs had ill-defined shapes (**Figure S1e**). The $Cu_3(PO_4)_2$ NS diffraction pattern is consistent with that of Hanawalt et. al (**Figure S1b**). The CuO NS and NPs were consistent with the tenorite crystal phase (**Figure S1d and f**). The CuO NP pattern shows nanoparticle texture with (002) reflection appearing more intense, which is consistent with preferential alignment on the zero-diffraction plate. Since particle morphology can directly determine dissolution and accumulation in plants Since particle differentiate shape and composition impacts on plant response.

In water, the dissolution of Cu^{2+} from $Cu_3(PO_4)_2$ NS in the first hour was 60-fold greater than CuO NPs and CuO NS (**Figure S2a**). Ion release from the $Cu_3(PO_4)_2$ NS plateaued at 400 mg/L (72-hour); a similar pattern of Cu gradual release from CuO NPs and CuO NS was evident,

although more was released from CuO NS (**Figure S2a**). Fumaric acid significantly altered Cu release from $Cu_3(PO_4)_2$ NS, which was 3-fold greater than in water during the first hour (**Figure S2b**). The Cu release pattern in fumaric acid from the different Cu NMs was similar to water, although the amounts were higher. Cu dissolution in sucrose was similar to water; $Cu_3(PO_4)_2$ NS released three times more ions than the other materials (**Figure S2c**). With proline, the rate of $Cu_3(PO_4)_2$ NS dissolution was increased, plateauing in the first hour at 9 mg/L; the other two forms only released 0.08-0.39 mg/L Cu^{2+} . CuO NP dissolution gradually increased over time but similar to the other solutions, remained low. Release from CuO NS increased rapidly and reached $Cu_3(PO_4)_2$ NS levels by day 7 (**Figure S2d**). This pattern of CuO NS dissolution in the proline solution was markedly different from the other solutions, indicating that both material morphology and solution properties are important. Faster dissolution of $Cu_3(PO_4)_2$ NS agrees with previous work. A P release from $Cu_3(PO_4)_2$ NS in the proline solution was 3 mg/L, which was 6-fold greater than in water, sucrose and fumaric acid (**Figure S2e**).

Cu²⁺ release was modeled using a combined density functional theory (DFT) and thermodynamics approach in which a Cu-OH unit is removed, in line with the mechanism determined for complex metal oxides. We hypothesize that the primary driving force for different Cu²⁺ release from the phosphate relative to the oxide is due to variable anions (O²⁻ or PO₄³⁻) in the lattice. To compare this anion effect, we model Cu²⁺ release from Cu₃(PO₄)₂ (ICSD#1143)²⁴ and CuO (ICSD#16025)²⁵. Starting positions and lattice constants were obtained from the Inorganic Crystal Structure Database (ICSD). From the relaxed bulk structures, (001) surfaces were cut and surface oxygens were protonated to maintain a charge balanced slab, as is appropriate based on stoichiometry and the experimental conditions (**Figure 1a and b**). The lattice effects are captured in ΔG_1 , which is the vacancy formation term calculated using equation 5, where lower ΔG_1 indicates more favorable release. The energy of releasing Cu-OH, including redox and hydration terms, is reported as ΔG_{tot} (**Figure 1c**).

 $\Delta G_1 = [E_{\text{Cu-OH vac}} + E_{\text{Cu(s)}} + E_{\text{O(g)}} + E_{\text{H(g)}}] - E_{\text{Pristine surface}}$ (5)

The hydrolysis of released Cu and ligand exchange reactions between dissolved Cu²⁺ and solution ions are accounted for to determine how media components influence dissolution (SI). These terms are added to ΔG_{tot} to obtain ΔG_{tot} +media (**Figure 1c**). ^{23, 26-28}

Cu dissolution was 60-fold greater from $Cu_3(PO_4)_2$ than from CuO NP and NS. All CuO Cu-OH surface units are equivalent, whereas $Cu_3(PO_4)_2$ has four different surface Cu-OH groups (equal molar quantities), labeled as $Cu_3(PO_4)_2$ -1 through -4, in different chemical environments (**Figure 1c**). $Cu_3(PO_4)_2$ -1 is chemically similar to the Cu-OH unit in CuO, circled in blue (**Figure 1b**), where an outermost Cu-OH group is removed. The phosphate material has a ΔG_{tot} that is 1.13 eV lower, indicating it is energetically more favorable to remove Cu-OH from $Cu_3(PO_4)_2$ -1. Removal of Cu-OH for $Cu_3(PO_4)_2$ -4 was energetically unfavorable as this unit is bound to phosphate that has a strong oxygen bond. Collectively, the modeling supports that Cu release from $Cu_3(PO_4)_2$ is thermodynamically favorable relative to CuO.

Dissolution experiments also showed media-dependent response where sucrose was similar to water, while fumaric acid and proline differentially increased Cu dissolution. Sucrose has the smallest effect on ΔG_{tot} (ΔG_{tot} +Sucrose), suggesting little impact on material dissolution. Fumarate caused an early increase in Cu release, supported by a relatively favorable ΔG_{tot} +Fumarate. For proline ligation to Cu, a square pyramidal structure of this complex was used,²⁹ resulting in the most energetically favorable ΔG_{tot} +media value, suggesting that proline greatly impacts dissolution. This is consistent with the experimental findings where proline increased dissolution by 1000-fold.

Response of infected soybean to Cu-based NM

For FV-infected plants, foliar exposure to Cu-based NMs stimulated soybean growth (Figure S3-5). However, there were no overt differences based on NMs type or dose. For the

healthy treatments, seedling size was unaffected by Cu-based NMs treatments (**Figure S3-5**). The root tissue in the FV control was severely infected by *Fusarium* as evident by black root rot; interestingly, foliar application of Cu-based NMs reduced the amount of infected root tissue (**Figure S4-5**).

FV infection reduced the shoot, root and nodule mass by 136, 60.6 and 93.4%, respectively (**Figure 2a-c**). Three sequential foliar applications of Cu-based NMs alleviated much of the FV-induced biomass reduction. CuO NS at 50 and 250 mg/L increased shoot biomass by 60.3% compared to the FV control; values approached the healthy controls (**Figure 2a**). Foliar CuO NS increased the mass of FV-infected roots by 34.3%; root and nodule mass in the diseased treatment was equivalent to healthy controls (**Figure 2b-c**). This alleviation of pathogen damage occurred with foliar addition of 2-3 mg of Cu during the seedling stage. Although an increasing trend of biomass was evident with Cu₃(PO₄)₂ NS and CuO NP, the effects were less robust than CuO NS. In the equivalent molar Cu treatments, trends for increased biomass were evident but statistical significance was infrequent due to replicate variability (**Figure S6a-c**). CuO NS significantly increased root biomass and had the largest nominal values in the other tissues. For the healthy treatments, exposure to Cu-based NMs had little impact on biomass (**Figure S6d-f**). In the ionic treatments, equivalent Cu²⁺ as CuSO₄ caused significant phytotoxicity (**Figure S6d-f**), whereas PO₄³⁻ increased the biomass of FV-infected shoots and nodules (**Figure 2a and c**).

FV infection decreased the net photosynthetic rate (Pn) by 43% (**Figure 2d**) but Cubased NMs at 50 and 250 mg/L alleviated this disease-induced reduction, restoring levels to healthy controls. In equivalent molar Cu treatments, effects were similar to the concentration-based data; disease-induced Pn and transpiration rate (Tr) reductions were alleviated (**Figure S7a-c**). In the ionic treatments, Cu²⁺ as CuSO₄ reduced Pn, Sc and Tr (**Figure S7d-f**) but PO₄³⁻ significantly increased photosynthetic efficiency (Pn, Tr) of infected plants, restoring levels to healthy controls (**Figure 2d and f**).

Tissue element content and distribution

Foliar amendment with Cu₃(PO₄)₂ NS, CuO NS and CuO NPs (50-250 mg/L) resulted in shoot Cu content that was 5.1-24-, 10-54-, and 6.8-34-fold greater than unamended controls, respectively (**Figure 3a**). CuO NS delivered 51.2-129% more Cu to shoots than the other two NMs (**Figure 3a**), although none of the amendments affected root Cu content (**Figure 3b**). FV infection increased shoot and root P content by 35.7 and 60.8%, respectively (**Figure 3c and d**), although Cu₃(PO₄)₂ NS did not impact the plant P content. In diseased roots, P levels were higher than healthy control across all treatments. In healthy plants, Cu accumulation in shoots and roots was similar to those with disease, including greater shoot Cu delivery with CuO NS (**Figure S8**). The P content of plants was not altered by Cu amendment, (**Figure S8**) suggesting that FV infection increases P accumulation in soybean. In the ionic treatments, high shoot Cu was noted and led to toxicity; P content was largely unaffected by phosphate amendment (**Figure 3d**). Additional nutritional elements were measured as a function of infection and nanoscale Cu treatments (**Table S1-4**); although some changes were evident as a function of *Fusarium* and/or Cu presence, no consistent effects were discernable.

SEM shows both Cu₃(PO₄)₂ NS and CuO NS on the leaf surface after treatment with 250 mg/L NM at harvest (< 3.5 mg Cu delivered) (**Figure 4b1-c1**). Although a greater amount of CuO NS appears to be retained on the surface, including by elemental mapping, Image J analysis shows no statistical difference (**Figure S9**). CuO NPs were not identified by EDS, which suggests less affinity for the leaf surface due to different particle morphology (**Figure 4s1**). No consistent pattern of spatial distribution was evident as a function of material type. Although **Figure 4a2-d2**, **S10** show no NMs around the trichomes, separate images do show particle presence near these structures.

Enzymatic and molecular response

Peroxidase (POD) and polyphenol oxidase (PPO) are antioxidant enzymes involved in plant response to stress.^{30, 31} POD activity in FV-infected shoots and roots was 3.51- and 1.84fold that of healthy controls; root POD activity was nearly 10-fold greater than levels in the shoot (Figure 5a and b). Cu-based NMs significantly decreased POD activity by 7-31.7% and 16.1-36% in infected shoots and roots, respectively (Figure 5a and b), suggesting reduced disease response due to enhanced innate resistance. CuO NS yielded the greatest reduction in POD activity, aligning with the above data and suggesting that overall defense stimulation is tunable as a function of material properties. A similar decreasing trend in POD activity was evident across all treatments with equivalent molar Cu, with CuO NS resulting in the lowest level (Figure S11a and b). PPO activity in FV-infected shoots was not significantly changed as compared to the diseased shoot controls (Figure 5c, S11c). The changes in PPO activity in FVinfected roots were similar to POD, although the treatment differences were of lesser magnitude (Figure 5d, S11d). CuO NS yielded the greatest decrease in root PPO activity relative to the other materials. For example, disease increased root PPO by 80%, but foliar CuO NS completely alleviated stress associated with infection and yielded PPO levels that were 30% less than the disease controls.

194

195

196

197

198

199

200

201

202

203

204

205

206

207

208

209

210

211

212

213

214

215

216

217

218

219

In the healthy treatments, Cu-based NMs had either no impact or decreased POD activity (Figure S11e and f). Some increases in PPO activity were evident in both shoots and roots upon treatment with Cu-based NMs, although not all were statistically significant (Figure S11g and h). With ionic Cu, a 52.3% increase in shoot POD was evident as compared to the FV control (Figure 5a), indicating that elevated Cu triggered antioxidant enzyme activity in response to metal-induced stress. Ionic Cu also elevated the shoot PPO levels by 83%; no difference was evident in roots (Figure 5c and d). With phosphate, POD and PPO activity were either decreased or unaffected in shoot and root tissues (Figure 5a-d).

Fatty acids are primary cell membranes and cutin wax components, functionally providing structural barriers and contributing to resistance against stress.^{32, 33} The fatty acid

profile in soybean tissues was investigated as a function of FV-infection and nanomaterial treatment. The total fatty acid content in the FV-infected shoot control was 50% less than the healthy controls (Figure S12a-b). CuO NS at 250 mg/L increased the total fatty acid content by 60.6% in FV-infected shoots compared to diseased controls, restoring levels to that of healthy plants (Figure S12a). The other Cu-based NMs also increased the total fatty acid content in FVinfected shoots, although variability among replicates precluded statistical significance (Figure S12a). Healthy shoots were unaffected by Cu-based NM treatments (Figure S12b). The total shoot fatty acid content in healthy treatments was relatively higher as compared to the diseased treated tissues. For example, the total shoot fatty acid content in the healthy treatments with Cu₃(PO₄)₂ NS and CuO NPs was significantly higher as compared to the corresponding diseased plants. In roots, the fatty acid content in the diseased and healthy controls were equivalent. However, foliar application Cu-based NMs elevated the total fatty acid content in the diseased roots as compared to the corresponding healthy roots (Figure S12c and d). Similar to infected shoots, the total fatty acid content in FV-infected roots was significantly increased by the Cu-based NM treatments by 10-44% (Figure S12c), while no difference was found in the Cu treated healthy roots (Figure S12d).

In plants under stress, unsaturated fatty acids (UFA) can be converted to saturated fatty acids (SFA); ^{34, 35} therefore, the ratio of SFA to UFA was evaluated. The ratio of SFA/UFA in FV-infected shoots was largely unchanged as compared to diseased shoot controls (**Figure S13a**); however, 250 mg/L Cu₃(PO₄)₂ NS and CuO NS did significantly increase in the SFA/UFA ratio in the roots (**Figure S13b**), indicating that foliar sheet-like Cu NMs amendment could trigger conversion of unsaturated to saturated fatty acids in FV-infected roots. In the equivalent molar Cu treatments, a common trend in shoots and roots was that the SFA/UFA ratio in the Cu-diseased treatment was higher that the corresponding Cu healthy treatment (**Figure S14a and b**), although the significance was weak due to replicate variability. For healthy treatments, different types of Cu-based NMs had slight impacts on the SFA/UFA ratio in both shoots and

roots (**Figure S14c and d**). Upon exposure to ionic Cu, the shoot SFA/UFA ratio was markedly higher than other treatments, suggesting Cu-induced phytotoxicity (**Figure S14c**).

246

247

248

249

250

251

252

253

254

255

256

257

258

259

260

261

262

263

264

265

266

267

268

269

270

271

Plants can remodel membrane fluidity by releasing phytooxylipin and α-linolenic acid (C18:3) in response to stress. $^{32, 36}$ Disease significantly reduced shoot α -linolenic acid (C18:3) content by several fold; however, foliar treatment with 250 mg/L CuO NS increased C18:3 content by 150% compared to disease controls (Figure S12a). CuO NS and CuO NPs also induced 11-92% increases in C18:3 content of treated shoots relative to diseased shoot controls. In healthy plants, Cu-based NMs decreased the C18:3 content 16% (Figure S12b), indicating that Cu-based NMs could induce membrane fluidity remodeling by stimulating C18:3 formation under healthy and diseased conditions. Notably, CuO NS exerted greater impact than did the other two NMs. In roots, changes in C18:3 induced by disease were largely reversed across all Cu treatments (Figure S12c and d), demonstrating the potential of foliar application of these materials to remodel root fatty acids profiles to strengthen plant defense. Treatment with 50 and 250 mg/L CuO NS increased the ratio of C18:3/(C18:0+C18:2) by 17% relative to the diseased control; 50 mg/L CuO NPs also significantly increased this shoot ratio (Figure S15a). Conversely, the root ratio in the CuO NS treatments was significantly lower relative to the diseased control, indicating the alleviation of FV-induced stresses in the root system. The equivalent molar Cu treatments exhibited similar trends in the C18:3/(C18:0+C18:2) ratio in FVinfected shoots and roots (Figure S16a and b). In healthy plants, the shoot ratio was largely unchanged, except with 250 mg/L CuO NS and 50 mg/L CuO NPs, which elevated the ratio by 7 and 11%, respectively (Figure S16c). Overall, foliar application of Cu-based NMs significantly altered both total fatty acid content and composition in diseased plants.

The expression of disease- and phytohormone-related genes in shoots and roots was analyzed. Hierarchical clustering analyses and principal component analyses (PCA) were performed to differentiate the impacts of Cu-based NMs in soybean (**Figure 6a-d**). CuO NS at both doses significantly changed pathogenesis (PR)-related genes in shoots, which were

markedly closer to the healthy control along PC1 (62.59%) (Figure 6b). PCA analysis for the PR genes in roots indicates that indirect exposure to Cu-based NMs induced less change, with treatments overlapping with the diseased control (Figure 6d). The relative expression of PR genes in the diseased shoot control was either upregulated or equivalent to the healthy shoot control (Figure S17a-f). However, exposure to Cu-based NMs downregulated PR genes in FVinfected shoots when compared to the corresponding disease control, nearly restoring levels to healthy controls (Figure S17a-d and f) and suggesting that foliar application of these materials could significantly counteract FV-induced stress and modulate plant defense response. A slight increase in NPR1 expression, which participates fungus-induced defense response, 37 in FVinfected shoots treated with Cu-based NMs (1.725 mM Cu) was evident (Figure S17g), indicating that NPR1 was less sensitive than PR genes or that up-regulation of other similar genes resulted in less need for NPR1. WRKY transcription factors modulate germination and development, biotic and abiotic stress response, and defense against pathogen infection. 38, 39, 40, ⁴¹ Upregulation of WRKY1 in the disease shoot control was evident (Figure S17h), and Cu₃(PO₄)₂ NS treatment further up-regulated WRKY1 expression by 4-fold, which is consistent with the PR findings from this treatment. Fan et al. (2017) demonstrated that WRKY and PR overexpression enhanced soybean resistance to *Phytophthora sojae*. Leucine-rich repeat (LRR) proteins can be activated upon fungal infection; significant upregulation of LRR in FVinfected shoots was evident across all Cu NM treatments (Figure S17i). In infected roots, similar trends in PR and disease-related gene expression were also found across all Cu-based NM treatments (Figure S18).

272

273

274

275

276

277

278

279

280

281

282

283

284

285

286

287

288

289

290

291

292

293

294

295

296

297

Antioxidant enzymes are also involved in the response to pathogen-induced stress. In the shoots, PPO-related gene expression in FV-infested plants was downregulated for nearly all Cu-based NM, except for CuO NPs at 50 mg/L (**Figure S17j-I**). The expression of phenylalanine ammonialyase (PAL) was downregulated for all treatments, except for Cu₃(PO₄)₂ and CuO NPs at 50 mg/L. In infected roots, there was significant upregulation (2-7-fold) of three antioxidant

defense-related genes with Cu-based NMs foliar exposure (**Figure S18**). Ma et al. (2019) also reported time-dependent upregulation defense related antioxidant genes in *Fusarium*-(FOL) infected tomato roots upon foliar exposure to Cu-based NMs; Cu₃(PO₄)₂ NS increased PPO and POD expression by 5-10 fold during the first 7 days of infection.¹⁴ The consistency across studies highlights the efficacy of foliar nanoscale Cu amendment as a strategy to modulate disease response, as well as the importance of particle properties at tuning that response.

298

299

300

301

302

303

304

305

306

307

308

309

310

311

312

313

314

315

316

317

318

319

320

321

322

Phytohormones are also sensitive indicators of abiotic and biotic stress. 43, 44 FV infection up-regulated most phytohormone-related genes in the shoots (Figure S19). However, the expression of auxin (AUX), gibberellin (GA2), cytokinin (CDHA6), salicylic acid (SAT) biosynthesis and dormancy-associated protein (DAP) genes were all downregulated with Cubased NMs (Figure S19a, b, d, f and h). Although jasmonate O-methyltransferase (JAT) expression in the diseased shoot was equivalent to the healthy control, Cu-based NMs increased JAT levels by 100% (Figure S19c). CuO NS increased the expression of strigolacton esterase (SLs) by 8-fold in diseased shoots; the other Cu NMs also induced upregulation to a lesser extent (Figure S19g). Abscisic acid (ABA) regulates aquaporin activity as abiotic stress response;⁴⁵ CuO NPs (1.725 mM Cu) increased ABA expression by 5-fold (Figure S19i). Phytohormone-related gene expression in the roots was similar to the shoots, with up-regulation in diseased tissue upon foliar nanoscale Cu (Figure S20). Root AUX was increased by 3-fold with Cu amendment (Figure S20a); CuO NS and CuO NPs (50 mg/L) increased root GA2 by 13- and 20-fold, respectively (Figure S20b). Similar trends were evident with infected root BR1, SAT, and DAP expression in upon Cu-based NMs treatment (Figure S20e, f and h). PCA analysis indicates that phytohormone-related genes were significantly altered in FV-infected shoots and roots (Figure S21). For example, CuO NS clearly separated in the diseased shoots and roots along with y axis; a lesser effect was also evident with Cu₃(PO₄)₂ NS (Figure S21b and d).

Engineered nanomaterials (ENMs) are known to alter the phytohormone network of terrestrial plants. Foliar exposure to nanoscale Fe₂O₃ and TiO₂ and carbon-based NMs increased the cytokinin zeatin riboside content in Turnip mosaic virus infected-tobacco by 40-100%; similar results were reported for BR content.⁴⁶ Hao et al. also reported that ENMs exposure inhibited *Podosphaera pannosa* infection in rose leaves by regulating phytohormone activity.⁴⁷ Although quantitative analysis of phytohormones has demonstrated their role in disease defense, little has been reported on the transcription levels of these regulatory genes upon infection and with Cu-based NMs. Our findings suggest that Cu-based NMs foliar exposure at the seedling stage significantly alters the expression of growth-related phytohormone genes, resulting in disease suppression and increased plant vigor over subsequent weeks of growth.

The expression of Cu, Zn and Fe transporters was measured in FV-infected shoots and roots (**Figure S22-23**). Although disease did not significantly alter these genes, modest upregulation was evident as a function of treatment. However, PCA analysis demonstrates little impact of disease or treatment on metal transporters (**Figure S24**); this data aligns with the elemental analysis, which also showed modest changes with disease and treatment (**Table S1-4**).

Conclusions

Foliar application of Cu-based NMs significantly suppressed FV infection in soybean as determined by phenotype, physiological parameters, photosynthetic endpoints and the transcription of several gene networks (**Figure S25**). CuO NS exhibited greater disease suppression than the other NMs; this activity correlates directly with material structure and dissolution, as determined experimentally and computationally. Elemental analysis shows that CuO NS delivered more Cu to the tissues, highlighting the importance of NM morphology and dissolution profile on leaf surface interactions and plant response. Fatty acid and molecular

- analyses indicate that Cu-based NMs, especially CuO NS, significantly alleviated FV-induced
- stress. Upon Cu treatment, the transcription of pathogenesis-related genes in FV-infected plants
- 351 largely returned to healthy control levels, demonstrating the role nanoscale Cu in disease
- response. The findings demonstrate that early seedling foliar application of small quantities of
- 353 nanoscale Cu offers great potential as a novel disease management strategy for soybean SDS.

354

355

References:

- 1. Lowry, G. V., Avellan, A., Gilbertson, L. M. Opportunities and challenges for nanotechnology in the agri-tech revolution. *Nature Nanotechnol.* **14.** 517 (2019).
- 2. Kah, M., Tufenkji, N., White, J. C. Nano-enabled strategies to enhance crop nutrition and protection. *Nature Nanotechnol.* **14,** 532 (2019).
- 360 3. Elmer, W., White, J. C. The future of nanotechnology in plant pathology. *Annu. Rev. Phytopathol.* **56**, *56*, 111-133 (2018).
- 362 4. Servin, A. et al. A review of the use of engineered nanomaterials to suppress plant disease and enhance crop yield. *J. Nanopart. Res.* **17**, 17 (2), 92 (2015).
- Bukovac, M., Wittwer, S. Absorption and mobility of foliar applied nutrients. *Plant Physiol.* **32**, 428 (1957).
- 366 6. Wang, Z. et al. Xylem-and phloem-based transport of CuO nanoparticles in maize (*Zea mays* L.). *Environ. Sci. Technol.* **46**, 4434-4441 (2012).
- 7. Rui, M.; Ma, C.; Hao, Y.; Guo, J.; Rui, Y.; Tang, X.; Zhao, Q.; Fan, X.; Zhang, Z.; Hou, T., Iron oxide nanoparticles as a potential iron fertilizer for peanut (Arachis hypogaea). *Front. Plant Sci.* **7**, 815 (2016).
- 371 8. Dimkpa, C. O. et al. Exposure to weathered and fresh nanoparticle and ionic Zn in soil promotes grain yield and modulates nutrient acquisition in wheat (*Triticum aestivum* L.). *J. Agr. Food Chem.* **66**, 66 (37), 9645-9656 (2018).
- Dimkpa, C. O., White, J. C., Elmer, W. H., Gardea-Torresdey, J. Nanoparticle and ionic Zn promote nutrient loading of sorghum grain under low NPK fertilization. *J. Agr. Food Chem.* **65**, 8552-8559 (2017).
- 10. Elmer, W. H.; White, J. C., The use of metallic oxide nanoparticles to enhance growth of tomatoes and eggplants in disease infested soil or soilless medium. *Environ. Sci. Nano* **3**, 1072-1079 (2016).
- 11. Elmer, W. et al. Effect of metalloid and metal oxide nanoparticles on Fusarium wilt of watermelon. Plant Dis. **102**, 1394-1401 (2018).
- Hao, Y. et al. Potential applications and antifungal activities of engineered nanomaterials against gray mold disease agent *Botrytis cinerea* on rose petals. *Front. Plant Sci.* **8**, *8*, 1332 (2017).
- 384 13. Borgatta, J. et al. Copper based nanomaterials suppress root fungal disease in watermelon (*Citrullus lanatus*): role of particle morphology, composition and dissolution behavior. *ACS Sustain. Chem.* 386 *Eng.* **6**, 14847-14856 (2018).
- Ma, C. et al. Time-dependent transcriptional response of tomato (*Solanum lycopersicum* L.) to Cu nanoparticle exposure upon infection with *Fusarium oxysporum* f. sp. *lycopersici. ACS Sustain. Chem. Eng.* **7**, 10064-10074 (2019).
- 390 15. Roy, K., Hershman, D., Rupe, J., Abney, T. Sudden death syndrome of soybean. *Plant Dis.* **81**, 391 1100-1111 (1997).
- 392 16. Aoki, T., O'Donnell, K., Homma, Y., Lattanzi, A. R. Sudden-death syndrome of soybean is caused by two morphologically and phylogenetically distinct species within the Fusarium solani species
- complex—*F. virguliforme* in North America and *F. tucumaniae* in South America. *Mycologia* **95**, 660-684 (2003).

- 17. Navi, S. S., Yang, X. Sudden death syndrome—a growing threat of losses in soybeans. *CAB Rev.* 397 **11.** 1 (2016).
- 398 18. Navi, S. S., Yang, X. Foliar symptom expression in association with early infection and xylem colonization by *Fusarium virguliforme* (formerly F. solani f. sp. glycines), the causal agent of soybean sudden death syndrome. *Plant Health Progr.* **9**, 24 (2008).
- 401 19. Hartman, G. L.; Chang, H.-X.; Leandro, L., Research advances and management of soybean sudden death syndrome. *Crop protection* **2015**, 73, 60-66.
- 403 20. Hanawalt, J., Rinn, H., Frevel, L. Chemical analysis by X-ray diffraction. *Ind. Eng. Chem. Anal.* 404 *Edition* **10**, 457-512 (1938).
- 405 21. Holder, C. F., Schaak, R. E. Tutorial on Powder X-ray Diffraction for Characterizing Nanoscale 406 Materials. *ACS Nano* **13,** 7359-7365 (2019).
- 407 22. Rong, X., Kolpak, A. M. Ab Initio Approach for Prediction of Oxide Surface Structure, 408 Stoichiometry, and Electrocatalytic Activity in Aqueous Solution. *J. Phys. Chem. Lett.* **6,** 1785-1789 409 (2015).
- 410 23. Bennett, J. W., Jones, D., Huang, X., Hamers, R. J., Mason, S. E. Dissolution of Complex Metal Oxides from First-Principles and Thermodynamics: Cation Removal from the (001) Surface of Li(Ni1/3Mn1/3Co1/3)O2. *Environ. Sci. Technol.* **52**, 5792-5802 (2018).
- 413 24. Shoemaker, G. L., Anderson, J. B., Kostiner, E. Copper(II) phosphate. *Acta Crystallogr. B* **33**, 414 2969-2972 (1977).
- 415 25. Asbrink, S., Norrby, L. J. A refinement of the crystal structure of copper(II) oxide with a discussion of some exceptional esd's. *Acta Crystallogr. B* **26**, 8-15 (1970).
- 417 26. Abbaspour-Tamijani A., et al. *DFT and Thermodynamics Calculations of Surface Cation Release* 418 *in LiCoO*₂. *Appli. Surf. Sci.* **515**, 145865 (2020).
- 419 27. Bennett, J. W., Jones, D. T., Hamers, R. J., Mason, S. E. First-Principles and Thermodynamics Study of Compositionally Tuned Complex Metal Oxides: Cation Release from the (001) Surface of Mn-421 Rich Lithium Nickel Manganese Cobalt Oxide. *Inorg. Chem.* **57**, 13300-13311 (2018).
- 422 28. Buchman, J. T. et al. Nickel enrichment of next-generation NMC nanomaterials alters material stability, causing unexpected dissolution behavior and observed toxicity to S. oneidensis MR-1 and D. magna. *Environ. Sci. Nano* **7**, 571-587 (2020).
- Bukharov, M. S. et al. Study of structural and dynamic characteristics of copper(ii) amino acid complexes in solutions by combined EPR and NMR relaxation methods. *Phys. Chem. Chem. Phys.* **16**, 9411-9421 (2014).
- 428 30. Pourcel, L., Routaboul, J. M., Cheynier, V., Lepiniec, L., Debeaujon, I. Flavonoid oxidation in plants: from biochemical properties to physiological functions. *Trends Plant Sci.* **12**, *12* (1), 29-36 (2007).
- 31. Bhaduri, A. M., Fulekar, M. Antioxidant enzyme responses of plants to heavy metal stress. *Rev. Environ. Sci. Bio.* **11,** 55-69 (2012).
- 432 32. Upchurch, R. G. Fatty acid unsaturation, mobilization, and regulation in the response of plants to stress. *Biotechnol. Lett.* **30**, 967-977 (2008).
- 33. Beisson, F., Li, Y., Bonaventure, G., Pollard, M., Ohlrogge, J. B. The acyltransferase GPAT5 is required for the synthesis of suberin in seed coat and root of Arabidopsis. *Plant Cell* **19**, 351-368 (2017).
- 436 34. Bonaventure, G., Salas, J. J., Pollard, M. R., Ohlrogge, J. B. Disruption of the FATB gene in Arabidopsis demonstrates an essential role of saturated fatty acids in plant growth. *Plant Cell* **15**, 1020-1033 (2003).
- 439 35. Peetla, C., Vijayaraghavalu, S., Labhasetwar, V. Biophysics of cell membrane lipids in cancer drug resistance: Implications for drug transport and drug delivery with nanoparticles. *Adv. Drug Deliver.* 441 *Rev.* **65**, 1686-1698 (2013).
- 442 36. Blée, E. Impact of phyto-oxylipins in plant defense. *Trends Plant Sci.* **7**, 315-322 (2002).
- 443 37. Backer, R., Naidoo, S., van den Berg, N. The nonexpressor of pathogenesis-related genes 1 (NPR1) and related family: mechanistic insights in plant disease resistance. *Front. Plant Sci.* **10**, 102 445 (2019).
- 38. Zhou, L. et al. Infection and genotype remodel the entire soybean transcriptome. *BMC Genomics* **10**, 49 (2009).
- 448 39. Mao, G. et al. Phosphorylation of a WRKY transcription factor by two pathogen-responsive MAPKs drives phytoalexin biosynthesis in Arabidopsis. *Plant Cell* **23**, 1639-1653 (2011).

- 450 40. Liu, Z. Q. et al. Cooperation of three WRKY-domain transcription factors WRKY18, WRKY40, and
- WRKY60 in repressing two ABA-responsive genes ABI4 and ABI5 in Arabidopsis. *J. Exp. Bot.* **63**, 6371-
- 452 6392 (2012).
- 453 41. Shanmugam, V. Role of extracytoplasmic leucine rich repeat proteins in plant defence 454 mechanisms. *Microbiol. Res.* **160**, 83-94 (2005).
- 455 42. Fan, S. et al. GmWRKY31 and GmHDL56 enhances resistance to *Phytophthora sojae* by regulating defense-related gene expression in soybean. *Front. Plant Sci.* **8**, 781 (2017).
- 457 43. Moradi, P., Ford-Lloyd, B., Pritchard, J. Metabolomic approach reveals the biochemical mechanisms underlying drought stress tolerance in thyme. *Anal. Biochem.* **527**, 49-62 (2017).
- 459 44. Blume, Y. B., Krasylenko, Y. A., Yemets, A. I. The Role of the Plant Cytoskeleton in Phytohormone Signaling under Abiotic and Biotic Stresses. *Mech. Plant Horm. Signaling Stress* 127-185 (2017) Editor: Pandey, G. K.
- 462 45. Yue, L., Ma, C., Zhan, X., White, J. C., Xing, B. Molecular mechanisms of maize seedling response to La₂O₃ NP exposure: water uptake, aquaporin gene expression and signal transduction. *Environ. Sci. Nano* **4**, 843-855 (2017).
- 465 46. Hao, Y. et al. Engineered nanomaterials suppress turnip mosaic virus infection in tobacco (Nicotiana benthamiana). *Environ. Sci. Nano* **5**, 1685-1693 (2018).
- 47. Hao, Y.; Fang, P.; Ma, C.; White, J. C.; Xiang, Z.; Wang, H.; Zhang, Z.; Rui, Y.; Xing, B., Engineered nanomaterials inhibit Podosphaera pannosa infection on rose leaves by regulating phytohormones. *Environ. Res.* **170**, 1-6 (2019).

Acknowledgements

471 472

481

482

- 473 This work was supported by the National Science Foundation under the Center for Sustainable
- 474 Nanotechnology, CHE-1503408. The CSN is part of the Centers for Chemical Innovation
- 475 Program. ICP-OES and ICP-MS work was supported by USDA-NIFA-AFRI 2016-67021-24985
- 476 and FDA 1U18FD005505-05, respectively. The computational portion of this work is was
- 477 supported by computational resources of the University of Iowa, Iowa City, Iowa, and by the
- 478 Extreme Science and Engineering Discovery Environment (XSEDE), which is supported by
- 479 National Science Foundation through allocation ID TG-GEO160006: Density Functional Theory
- 480 Calculations for Nanomaterials in Energy Applications and the Environment.

Author contributions

- 483 C.M. and J.C.W. designed the experiment. C.M. conducted greenhouse experiment. J.B. and
- 484 R.J.H provided Cu₃(PO₄)₂ and CuO nanosheets. B.G.H., A.A.T. and S.E.M. conducted periodic
- 485 DFT calculations. R.D.L.T.R., N.Z.M. and Y.S. helped with plant maintenance in greenhouse.
- 486 W.H.E. provided Fusarium millet and technical support for Fusarium infection. B.X. provided
- technical support for fatty acid analysis using GC-MS and provided greenhouse resources. C.M.

488 and J.C.W. wrote the manuscript. C.M., R.J.H. and J.C.W revised the manuscript. All authors 489 discussed the results and commented on the manuscript. 490 491 **Additional information** 492 Extended data that includes separate replicated experiments and a demonstration of 493 repeatability of findings are available with the online version of this paper. In addition, 494 supplementary information is available in the online version of the paper. Reprints and 495 permissions information is available online at www.nature.com/reprints. Correspondence and 496 requests for materials should be addressed to J.C.W. 497 498 **Competing interests** 499 The authors declare no completing interests. 500 501 **ORCID** 502 Chuanxin Ma: 0000-0001-5125-7322 503 Jaya Borgatta: 0000-0002-9381-6097 504 Blake Hudson: 0000-0003-0675-1772 505 Ali Abbaspour Tamijani: 0000-0003-4867-0487 506 Roberto De La Torre-Roche: 0000-0001-7370-4373 507 Nubia Zuverza-Mena: 0000-0003-2721-7691 508 Wade H. Elmer: 0000-0003-3308-4899 509 Baoshan Xing: 0000-0003-2028-1295 510 Sara Mason: 0000-0003-1515-6780 511 Robert J. Hamers: 0000-0003-3821-9625 512 Jason C. White: 0000-0001-5001-8143 513

514

Methods

Cu-based nanomaterials CuO NPs (40 nm) were obtained from US Research Nanomaterials Inc. (Houston, TX). All reagents were used without further purification. The reagents obtained from Millipore Sigma were CuCl₂·2H₂O, LiOH·H₂O, diethylene glycol, and ammonium phosphate. Copper phosphate nanosheets were synthesized using previously reported methods.^{13, 19} Briefly, 20 mL of diethylene glycol was heated to 140 °C under reflux. Four mL of 1.875 M aqueous CuCl₂·2H₂O was then added dropwise to the heated diethylene glycol, and the solution was stirred for 45 min. The temperature was then increased to 180 °C and 4 mL of 1.25 M ammonium phosphate solution was rapidly injected using a syringe. The reaction continued for 5 hours more. The particles were then isolated using centrifugation (5000 rpm for 10 min, Thermo scientific Sorvall). The particles were rinsed with ethanol, re-suspended using a vortex (VWR standard mini Vortex), and isolated using centrifugation (5000 rpm for 10min). The rinsing protocol was repeated with ethanol and water. The particles were then allowed to dry overnight under vacuum. The hydrothermal synthesis of CuO nanosheets was adapted from Su et al. Briefly, 8 mmol of CuCl₂·2H₂O was dissolved in 160 mL of nanopure water (18.2 mΩ, Thermo Fisher Barnstead systems).⁴⁸ Twenty-four mmol of LiOH was then

added to the solution. The reaction was stirred for 10 minutes, then transferred to an autoclave (Parr instruments). The reaction was heated to 170 °C for 2 h. The reaction was then allowed to cool to ambient temperature. The particles were then isolated, cleaned and dried as previously described.

The materials were characterized by X-ray diffraction and scanning electron microscopy. A Bruker D8 powder diffractometer was used to determine the diffraction patterns of $Cu_3(PO_4)_2 \cdot 3H_2O$ nanosheets, CuO nanosheets and CuO nanoparticles. To prepare each sample the nanoparticles or nanosheets were pressed into vacuum grease on a zero-diffraction silicon wafer (MTI corporation). Scanning electron microscopy was used to determine the nanoparticle morphology. To prepare each sample, the nanoparticles were suspended in ethanol and sonicated using a bath sonicator (Branson 2510). The nanoparticle suspensions were then drop-casted on to silicon wafers. The samples were analyzed using a LEO Supra55 VP field-emission scanning electron microscope.

Periodic DFT calculations were carried out using QUANTUM ESPRESSO suite⁴⁹ along with GBRV ultrasoft pseudopotentials.⁵⁰ A planewave cutoff of 40 Ry and a charge density cutoff of 320 Ry was selected. The reciprocal space was sampled using a 3×3×1 grid of *k*-points for both CuO and Cu₃(PO₄)₂. Molecular calculations, including spin polarization effects, were performed using DMol³ software as implemented in BIOVIA Materials Studio package.⁵¹ Dispersion effects were accounted for via Grimme correction scheme.⁵² This scheme has been demonstrated to perform well in a variety of systems prior to the present study.⁵³ DNP basis sets were used alongside a global cutoff radius of 4.50 Å. The molecular calculations were performed in an implicitly solvated environment, with a dielectric constant of 78.54 for water. The solvated environment feature was invoked through the COnductor-like Screening MOdel, known as COSMO.⁵⁴⁻⁵⁵ Atoms in all calculations were relaxed to within 5 meV/atom, and used the GGA-PBE exchange-correlation functional.⁵⁶ Ligand exchange reactions that model the

media effects and Figures depicting their presumptive products are all included in **Figure S25A- E**.

Dissolution experiment Cu²+ release from Cu₃(PO₄)₂ nanosheets, CuO nanosheets, and CuO nanoparticles was evaluated in deionized water and in solutions containing sucrose, fumaric acid or proline; these analytes represent the dominant sugar, organic acid and amino acid in phloem sap, respectively (pH 7.5).⁵⁷ The amounts of three Cu-based nanomaterials were normalized by the equivalent molar Cu concentration (0.69 mM) and were separately prepared in 40 mL deionized water, 65.89 mM sucrose, 4.16 mM fumaric acid, and 18.28 mM proline. All suspensions were ultra-sonicated for 1 min and then shaken at 200 rpm at ambient temperature. Samples were collected at 1, 6, 12, 24, 72 and 168 h. Three replicates were used in each treatment at each time point. Centrifugal ultrafiltration devices (3000 dalton, UFC900396, MilliporeSigmaTMAmiconTM) were used to separate particulates from the filtrate with the dissolved ions at 4000 rpm for 20 min. The collected filtrate was acidified by concentrated HNO₃ prior to quantitation of Cu and P by ICP-MS (Agilent 7500ce) and ICP-OES (iCAP 6500) as noted below.

Greenhouse experiment The soybean cultivar 'Seedranch' (Seedranch, Odessa, FL) was used to test the efficiency of Cu-based nanomaterials for disease suppression through nutritional modulation. Soybean seeds were surface-sterilized with 70% (*v/v*) ethanol, rinsed with deionized water several times, and air-dried on a paper towel prior to seeding. To facilitate nodule formation, seeds were inoculated with Rhizobium. The *F. virguliforme* (Isolate Mont-1; FV) inoculum was prepared as described by Elmer and White. Briefly, *F. virguliforme*-colonized semi-solid agar medium was seeded into Japanese millet, which was autoclaved with deionized water (1:1 *w/v*) for 1 hour. The culture was allowed to grow for 2 weeks at 22–25 °C and then the inoculated millet was air-dried and ground into fine powder before use. The

inoculum concentration was 2 g/L soilless potting mix (ProMix BX, Premier Hort Tech, Quakertown, PA, USA). The soybean seeds were germinated in FV-amended potting mix; seeds germinated in potting mix without the FV amendment were set as pathogen-free controls (healthy treatments). Sterile millet was not added to the healthy treatments because it was previously shown to have no effect on plant growth.⁵⁸ All plants were maintained under greenhouse conditions (temperature: 25 °C; relative humidity: 74%; light period: 16/8, day/night).

602

603

604

605

606

607

608

609

610

611

612

613

614

615

616

617

618

619

620

621

622

623

624

625

626

627

Seven-day old soybean seedlings of uniform size were foliar-amended with different concentrations of Cu-based nanomaterials (NMs) using a "plant dip" procedure described previously. 13 NM suspensions of Cu₃(PO₄)₂·3H₂O nanosheets, CuO nanosheets, and commercial CuO nanoparticles (NPs) were prepared in deionized water amended with a nonionic surfactant (Regulaid®, 1 ml/L) to facilitate solution retention on the leaves. The CuO NP suspension was sonicated using a probe sonicator for 5 min in an ice bath. Because of concern over material damage, Cu₃(PO₄)₂·3H₂O and CuO NS suspensions were sonicated using a bath sonicator for 1 min. NM solution concentrations of 50 and 250 mg/L were used for the foliar dip; in separate replicates, the concentration of Cu-based NMs was also normalized by the same Cu molar concentration (the molar concentration of Cu in 250 mg/L Cu₃(PO₄)₂·3H₂O is 1.725 mM). Ionic controls included CuSO₄·5H₂O and Na₃PO₄·12H₂O for Cu²⁺ (1.725 mM) and PO₄³⁻ (1.125 mM), respectively. The healthy and diseased controls were foliar-treated with deionized water amended with 1 mL/L nonionic surfactant. For foliar treatment, individual soybean seedlings were inverted into the appropriate suspension for approximately 10 seconds, then allowed to air-dry for approximately 60 min to avoid the possible contamination to the substrates prior to transplanting into a plastic pot containing potting mix w/ or w/o FV. The seedlings across all treatments were foliar-treated with the NM suspensions three times within a 7-day interval (Day 0, Day 7, Day 14). An estimate of total volume of 1.5 mL of NM suspension was retained on each seedling, resulting in the delivery of approximately 0.75-3.75 mg of Cu NM per application. All seedlings were randomly arranged on greenhouse bench and were

watered with the same volume of tap water each day. After 40 days, phenotypic images of both soybean shoots and roots were taken to qualitatively evaluate the FV-induced damages to plant tissues as a function of different types of Cu-based NMs. In addition, fresh biomass (n=5) was recorded across all the treatments at harvest. All plant tissues were stored at -80 °C until further analysis. Seedlings across all the treatments were separate into shoots (leaves and stems) and roots. Then, the individual shoot and root parts were ground into fine powder in liquid nitrogen using a set of autoclaved mortar and pestle, which were clean with ethanol between samples to avoid the possible DNA or RNA contaminations. The ground tissues were used for the measurements of element content, antioxidant enzymes activity, fatty acids profile, and transcriptomic analysis.

Photosynthesis measurement

Prior to harvest, the photosynthetic efficiency of soybean leaves was measured across all treatments. A leaf in the same position on each seedling was selected to measure photosynthesis rate (Pn), stomatal conductance (Sc) and transpiration rate (Tr) using LI–6400XT Portable Photosynthesis System (LI-COR Biosciences). For instrument conditions, the CO_2 in reference chamber was fixed at 400 µmoles; the relative humidity was between 50–65%; the light intensity was 750 µmoles; and the flow was 200 µmoles. The instrument was recalibrated every fifteen samples in order to obtain stable readings.

Element measurement

Fresh soybean shoot and root tissues across all the treatments (n=4) were separately ground into a fine powder in liquid nitrogen. A portion of ground tissues was transferred into a 50 mL digestion tube for freeze-drying in a lyophilizer (FreeZone 2.5 Liter-50C, Labconco, Kansas City, MO). The weight of freeze-dried shoot tissues across all the treatments ranged from 100 to 200 mg; and the root dry weight ranged from 20-50 mg. The shoot and root tissues

were separately digested using a two-step protocol prior to elemental analysis. Briefly, freezedried tissues amended with 3 mL of concentrated HNO $_3$ were heated at 115 °C for 40 min on a heat block (DigiPREP System; SCP Science, Champlain, NY). The digest was cooled down at ambient temperature and 0.5 mL of H_2O_2 was added prior to another 20 min of digestion at 115 °C. The content of both macro- and micronutrients was measured using inductively coupled plasma optical emission spectroscopy (ICP-OES; iCAP 6500; Thermo Fisher Scientific, Waltham, MA). In addition, the root Cu content was measured by inductively coupled plasma mass spectrometry (ICP-MS, Agilent Technologies 7500ce, Santa Clara, CA, USA). Individual elemental concentrations were calculated as mg/kg dry weight.

Nanomaterial imaging on leaf surfaces

Representative soybean leaf tissues from the 250 mg/L NM treatments and the equivalent molar Cu concentration treatment were sampled after the third dosing. All the tissues were frozen in liquid nitrogen and freeze-dried by a lyophilizer. The samples were mounted onto carbon sticky tape and gold coated for 90 seconds using an SPI sputter coater (Westchester, PA) with a discharge current of 18 mM using argon gas. The distribution of Cu₃(PO₄)₂·3H₂O nanosheets, CuO nanosheets, and commercial CuO NPs on soybean leaf tissues was observed using a Leo Supra V55 scanning electron microscope (SEM), with an accelerating voltage of 1 eV, and with a Thermo Scientific energy dispersive X-ray spectroscopy detector (EDS) at an accelerating voltage of 20 eV.

Antioxidant enzyme content

Peroxidase (POD) and polyphenol oxidase (PPO) activity were measured in soybean roots and shoots across all treatments (n=4) as described in Ma et al.⁵⁹ The enzymes were extracted in 50 mM phosphate (pH7.0) amended with 1% (w/v) polyvinylpyrrolidone. For POD measurement, 50 µL of root enzyme extract or 100 µL of shoot enzyme extract was mixed with

1.85 mL or 1.80 mL of reaction buffer (0.2% guaiacol in 50 mM sodium phosphate buffer, pH 7.0) in a cuvette, respectively. Then 0.1 mL of 1% (ν/ν) H₂O₂ was added to initiate the reaction. The increased absorbance was recorded at 470 nm for 30 sec.⁶⁰ For PPO measurement, 200 μ L of root/shoot enzyme extract was mixed with 1.8 mL of 10 mM catechol prepared in 50 mM phosphate buffer (pH 7.0). The increased absorbance was recorded at 398 nm every 20 second over 1 minute.^{60, 61}

686

687

688

689

690

691

692

693

694

695

696

697

698

699

700

701

702

703

680

681

682

683

684

685

Fatty acid profile

Approximately 0.2-0.3 g of frozen shoot and root fine powders was weighed into 15 mL conical tubes containing 2.5 mL of methanol acidified by H₂SO₄ (2.5%, v/v). Three biological replicates were applied in each treatment. All samples were derivatized at 80 °C for 1 h and then cooled down to ambient temperature. Two mL of deionized water and 3 mL of hexane were added, followed by vigorous shaking for 30 min to extract fatty acid methyl esters (FAMEs). The extract was separated from water phase by centrifugation at 3000 rpm for 5 min. 62 The extraction step was repeated once to ensure an adequate recovery. The collected extract was concentrated under N2 and then re-suspended in 2 mL (root) or 5 mL (shoot) of dichloromethane (CH₂Cl₂). FAMEs analysis was done by gas chromatography-mass spectrometry (GC-MS; GCMS-QP2010 Ultra, Shimadzu, Kyoto, Japan) using an integrated guard column (Rtx-5MS, 30 m in length, 0.25 mm in diameter, 0.25 µm in thickness, Shimadzu, Kyoto, Japan). The sample injection volume was 1 µL under splitless mode with helium carrier gas. The injection, ion-source, and interface temperature were 250, 200, and 300 °C, respectively. The thermal program was as follows: the column oven temperature was at 80 °C and increased at 3 °C/min to 290 °C. spectra were recorded within a m/z range from 40 to 450. FAMEs standard compounds were purchased from AccuStandard, Inc. (New Haven, CT).

704

705

Transcriptomic analysis

Fresh shoot and root tissues were ground into fine powder in liquid nitrogen. Approximately 100 mg of fresh tissue was weighed into a 1.5 mL Eppendorf tube for total RNA isolation using a Sigma-Aldrich Spectrum Plant Total RNA Kit (Sigma-Aldrich, St. Louis, MO). The concentration and quality of the isolated total RNA samples were measured by a Thermo Scientific Nanodrop Lite Spectrophotometer (Thermo Fisher Scientific, Wilmington, DE). A Verso cDNA synthesis kit was used to synthesize complementary DNA using 1 µL of total RNA as a template. The gene-specific primers were designed using the PrimerQuest Tool (Integrated DNA Technologies, Coralville, IA) and the working concentration of each primer was 10 µM. A list of all genes involved in plant resistance, phytohormones, metal transporters, and nitrogen assimilation is provided in Table S5. Reverse-transcription real-time PCR (RT-qPCR) was performed with the Bio-Rad SsoAdvanced Universal SYBR Green Supermix (Bio-Rad, Hercules, CA) using the Bio-Rad CFX96 Touch Real-Time PCR Detection System (Bio-Rad). The synthesized cDNA was diluted to 50 ng/µL with double distilled water. One microliter of the diluted cDNA was used as template for qPCR analysis. The thermal program for qPCR amplification was 95 °C for 30 s; 95 °C for 15 s, 62 °C for 30 s, repeating 40 cycles; melting curve from 65 °C to 95 °C. The relative expression of each gene was calculated by 2-ΔΔCt method using EF1b as the housekeeping gene. Gene fold-change was expressed relative to the FV control plants.

724

725

726

727

728

729

730

706

707

708

709

710

711

712

713

714

715

716

717

718

719

720

721

722

723

Data analysis

The experiment was arranged on greenhouse benches as a complete randomized design with 5 replicates per treatment. Data sets were subjected to Shapiro-Wilk's W Test of homogeneity before an ANOVA was performed. A Mixed Model one-way ANOVA procedure was used with NP treatments as fixed effects and experimental repetition, and replicates as random effects. Means were separated using Duncan's Multiple Range Test at P = 0.05. All

- analyses were performed using SPSS statistics (Version 26, IBM Corp., Armonk, New York,
- 732 United States).

733

734 Data Availability

- Additional data related to this paper is available from the corresponding author upon reasonable
- 736 request.

737

738

References

- 48. Su, D., Xie, X., Dou, S., Wang, G. CuO single crystal with exposed {001} facets--a highly efficient material for gas sensing and Li-ion battery applications. *Sci. Rep.* **4**, 5753 (2014).
- Giannozzi, P.et al. QUANTUM ESPRESSO: a modular and open-source software project for quantum simulations of materials. *J. Phys. Condens. Matter* **21**, 395502 (2009).
- Garrity, K. F., Bennett, J. W., Rabe, K. M., Vanderbilt, D. Pseudopotentials for high-throughput DFT calculations. *Comput. Mater. Sci.* **81.** 446-452 (2014).
- Delley, B. From molecules to solids with the DMol3 approach. *J. Chem. Phys.* **113**, 7756-7764 (2000).
- 747 52. Grimme, S., Antony, J., Ehrlich, S., Krieg, H. A consistent and accurate ab initio parametrization of density functional dispersion correction (DFT-D) for the 94 elements H-Pu. *J. Chem. Phys.* **132**, 154104 (2010).
- 750 53. Tamijani, A. A., Salam, A., de Lara-Castells, M. P. Adsorption of Noble-Gas Atoms on the TiO2(110) Surface: An Ab Initio-Assisted Study with van der Waals-Corrected DFT. *J. Phys. Chem. C* **120**, 18126-18139 (2016).
- 753 54. Klamt, A.; Schüürmann, G. COSMO: a new approach to dielectric screening in solvents with explicit expressions for the screening energy and its gradient. *J. Chem. Soc. Perkin Trans.* **2**, 799-805 (1993).
- 756 55. Andzelm, J., Kölmel, C., Klamt, A. Incorporation of solvent effects into density functional calculations of molecular energies and geometries. *J. Chem. Phys.***103**, 9312-9320 (1995).
- 758 56. Perdew, J. P.; Burke, K.; Ernzerhof, M., Generalized Gradient Approximation Made Simple. *Phys.* 759 *Rev. Lett.* **77**, 3865-3868 (1996).
- 760 57. Hijaz, F., Killiny, N. Collection and chemical composition of phloem sap from Citrus sinensis L. Osbeck (sweet orange). *PloS One* **9**, e101830 (2014).
- 762 58. Perez, C. D. P. et al. Metalloid and Metal Oxide Nanoparticles Suppress Sudden Death Syndrome of Soybean. *J. Agric. Food Chem.* **68**, 77-87 (2020).
- 764 59. Ma, C. et al. Defense mechanisms and nutrient displacement in Arabidopsis thaliana upon exposure to CeO₂ and In₂O₃ nanoparticles. *Environ. Sci. Nano* **3**, 1369-1379 (2016).
- 766 60. Jing, G.et al. Effect of pyrogallol on the physiology and biochemistry of litchi fruit during storage. 767 *Chem. Cent. J.* **7**, 19 (2013).
- 61. Su, M. et al. Physical changes and physiological characteristics of red and green peel during nectarine (cv. Hu018) maturation. *J. Sci. Food Agri.* **92**, 1448-1454 (2012).
- To be described to the first section of the first s

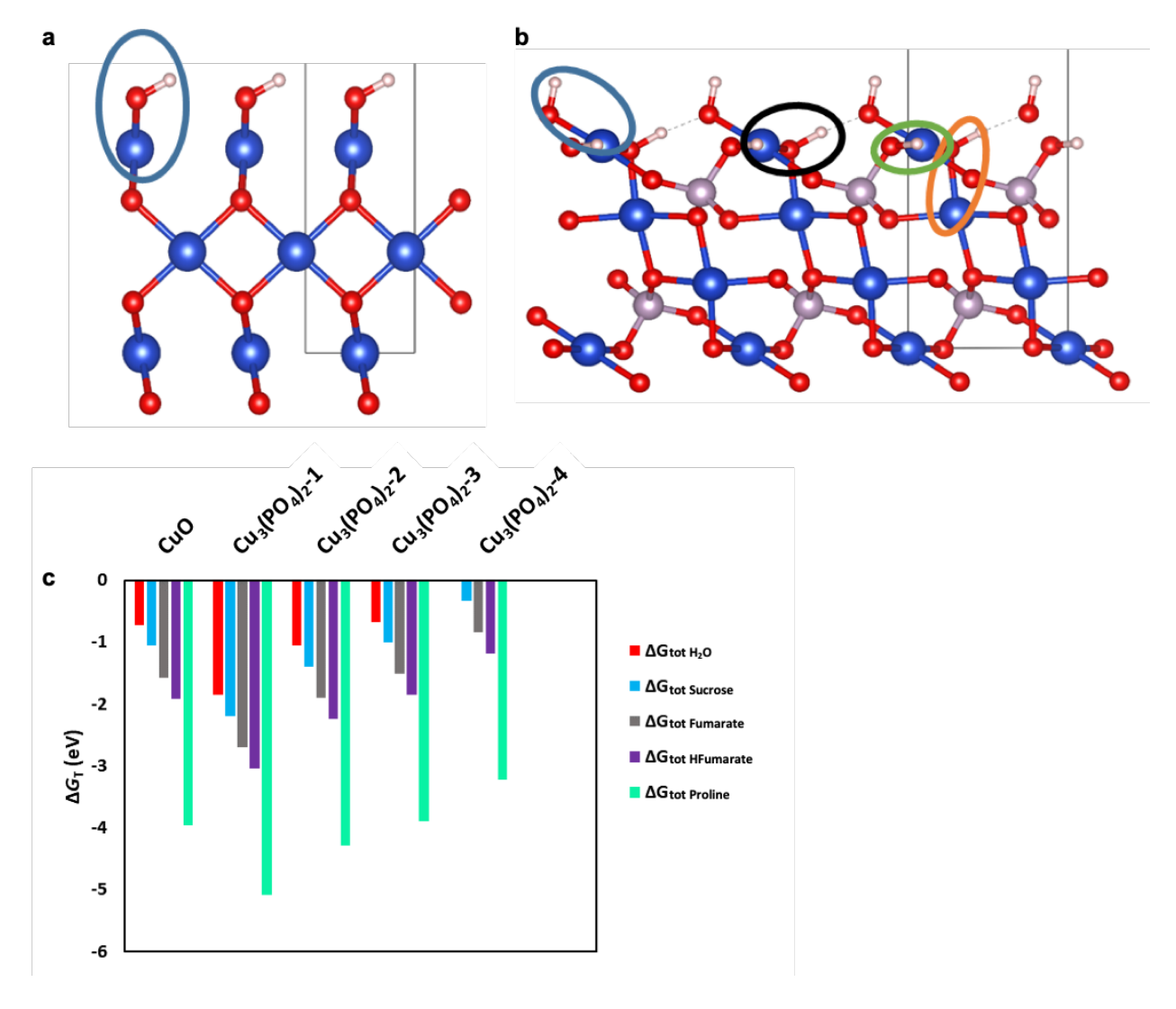


Figure 1. (a) Side view of CuO with only one Cu-OH unit to remove. (b) Side view of $Cu_3(PO_4)_2$ showing there are four inequivalent Cu-OH sites. (1, blue) The topmost unit with a labile -OH bound to surface Cu. (2, black) -OH shared between two coppers where the surface Cu is removed. (3, orange) Same -OH as 2 where the bulk-like Cu is removed instead. (4, green) OH shared between surface copper and phosphate. Grey lines are added for visual guidance. (c) the ΔG_{tot} values of Cu-OH removals (red) relative to $Cu_3(PO_4)_2$ -4. Media effects are added to these numbers to yield ΔG_{tot} +media for Sucrose (blue), Fumarate (grey), HFumarate (purple), and Proline (green).

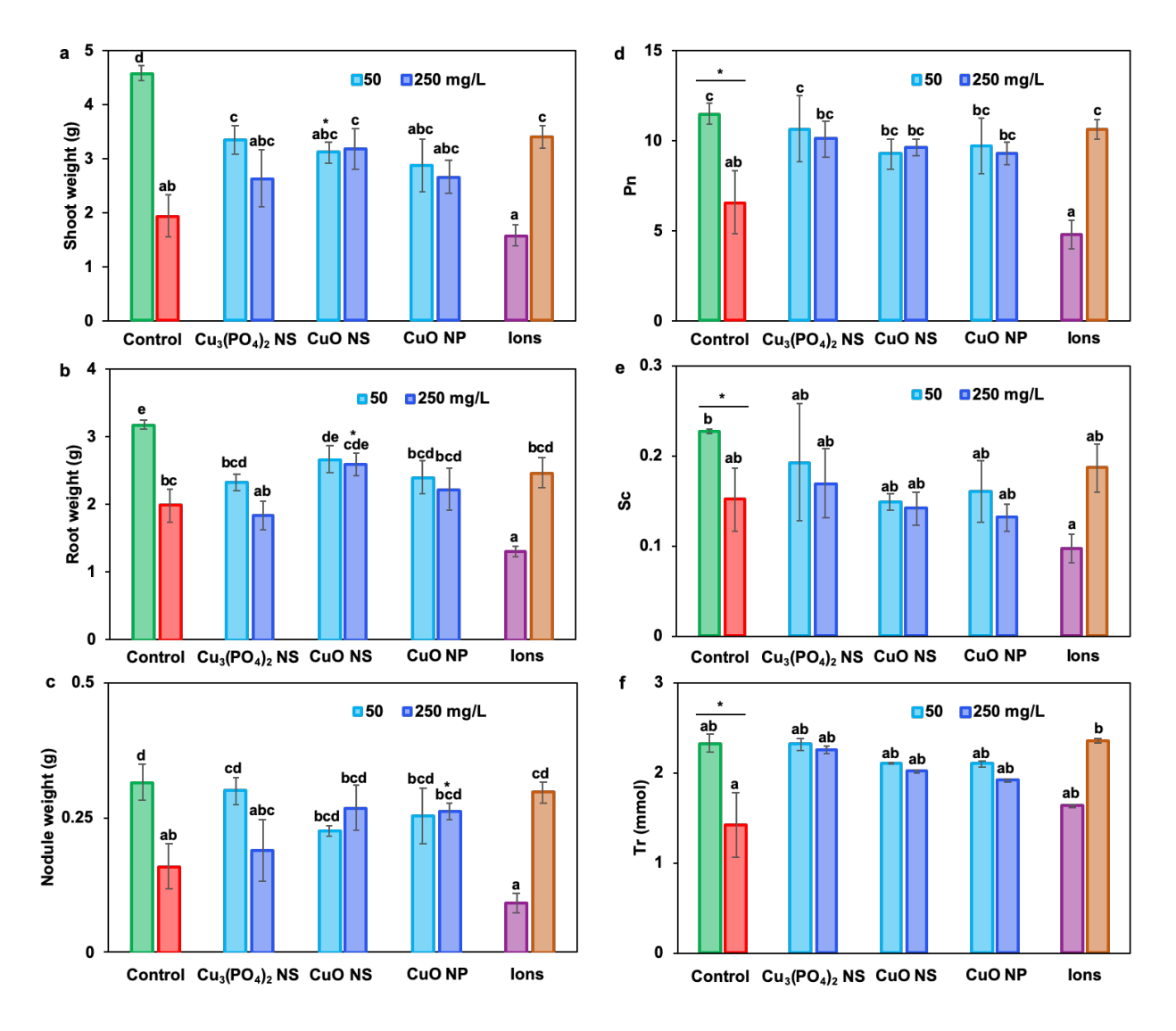


Figure 2. Physiological responses of FV infected soybean upon foliar-exposure to different types of Cu-based NMs. Figure a-c shows fresh biomass of shoots, roots and nodules, respectively, in the FV treatments with different types of Cu-based NMs at 50 and 250 mg/L (mass of particles); Figure d-f represents net photosynthetic rate, stomatal conductance and transpiration rate, respectively, in the FV treatments with different types of Cu-based NMs at 50 and 250 mg/L (mass of particles). In each panel, green bar (□) and red bar (□) represents healthy control and diseased control, respectively; blue bars represent the treatments with different types of Cu-based NMs at 50 and 250 mg particles/L; purple bar (□) and brown bar (□) represents 1.725 mM [Cu] ionic control and 1.175 mM [PO₄³-] ionic control, which is the same molar concentration of [Cu] and [PO₄³-] in 250 mg/L Cu₃(PO₄)₂ NS, respectively. In Figure a-c, error bars correspond to standard error of mean (n=5); single asterisk "*" indicates significant difference between the diseased control and each Cu-based NM treatment at p<0.05. In Figure d-f, error bars correspond to standard error of mean (n=3); single asterisk "*" indicates significant difference between the healthy and the diseased control at p<0.05. Values followed by different letters are significantly different at p<0.05.

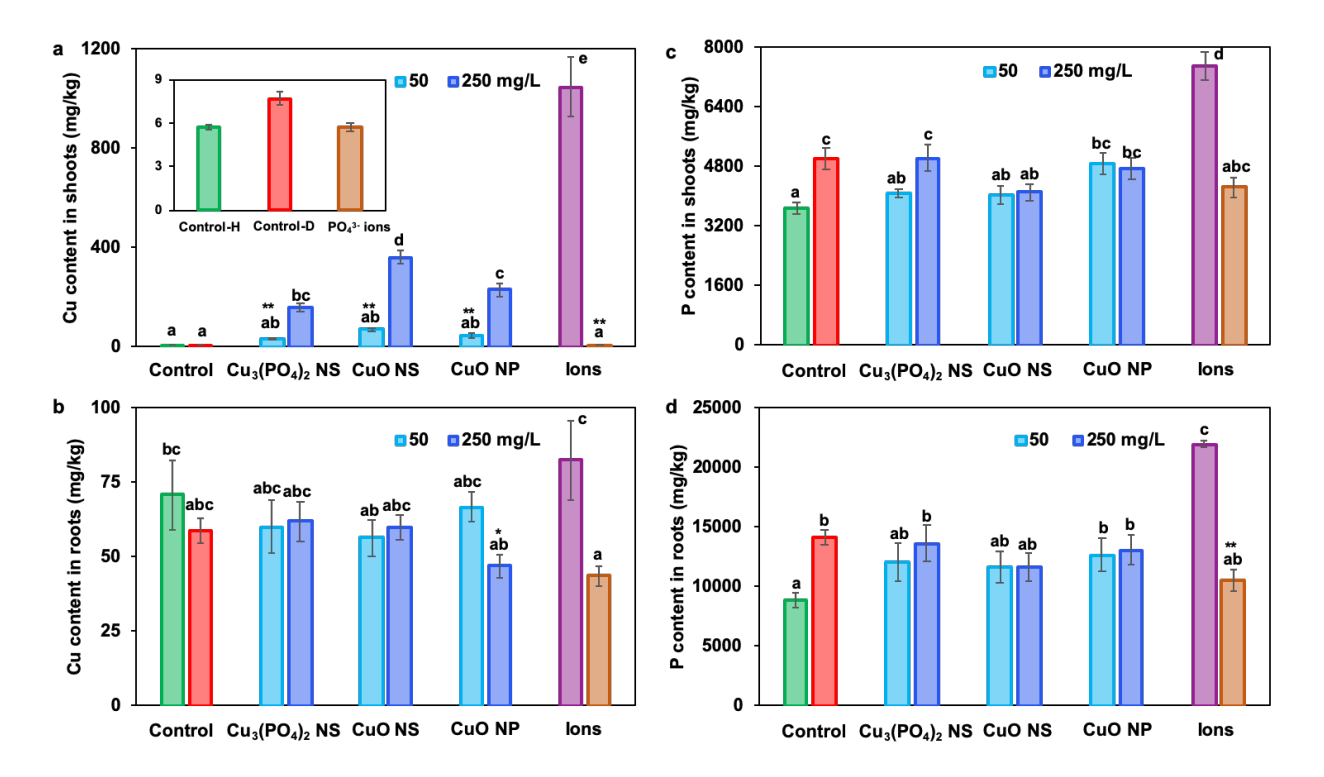


Figure 3. Cu and P content of FV infected soybean upon foliar-exposure to different types of Cubased NMs. Figure a-b shows the Cu content in shoots and roots, respectively, in the FV treatments with different types of Cu-based NMs at 50 and 250 mg/L (mass of particles); Figure c-d represents the P content in shoots and roots, respectively, in the FV treatments with different types of Cu-based NMs at 50 and 250 mg/L (mass of particles). In each panel, green bar (□) and red bar (□) represents healthy control and diseased control, respectively; blue bars represent the treatments with different types of Cu-based NMs at 50 and 250 mg particles/L; purple bar (□) and brown bar (□) represents 1.725 mM [Cu] ionic control and 1.175 mM [PO₄³⁻] ionic control, which is the same molar concentration of [Cu] and [PO₄³⁻] in 250 mg/L Cu₃(PO₄)₂ NS, respectively. Error bars correspond to standard error of mean (n=4); values followed by different letters are significantly different at p<0.05. In addition, in each panel, single asterisk "*" indicates significant difference between the diseased control and each Cu-based NM treatment at p<0.05; double asterisks "**" indicate significant difference between the diseased control and each Cu-based NM treatment at p<0.01 using a student t-test.

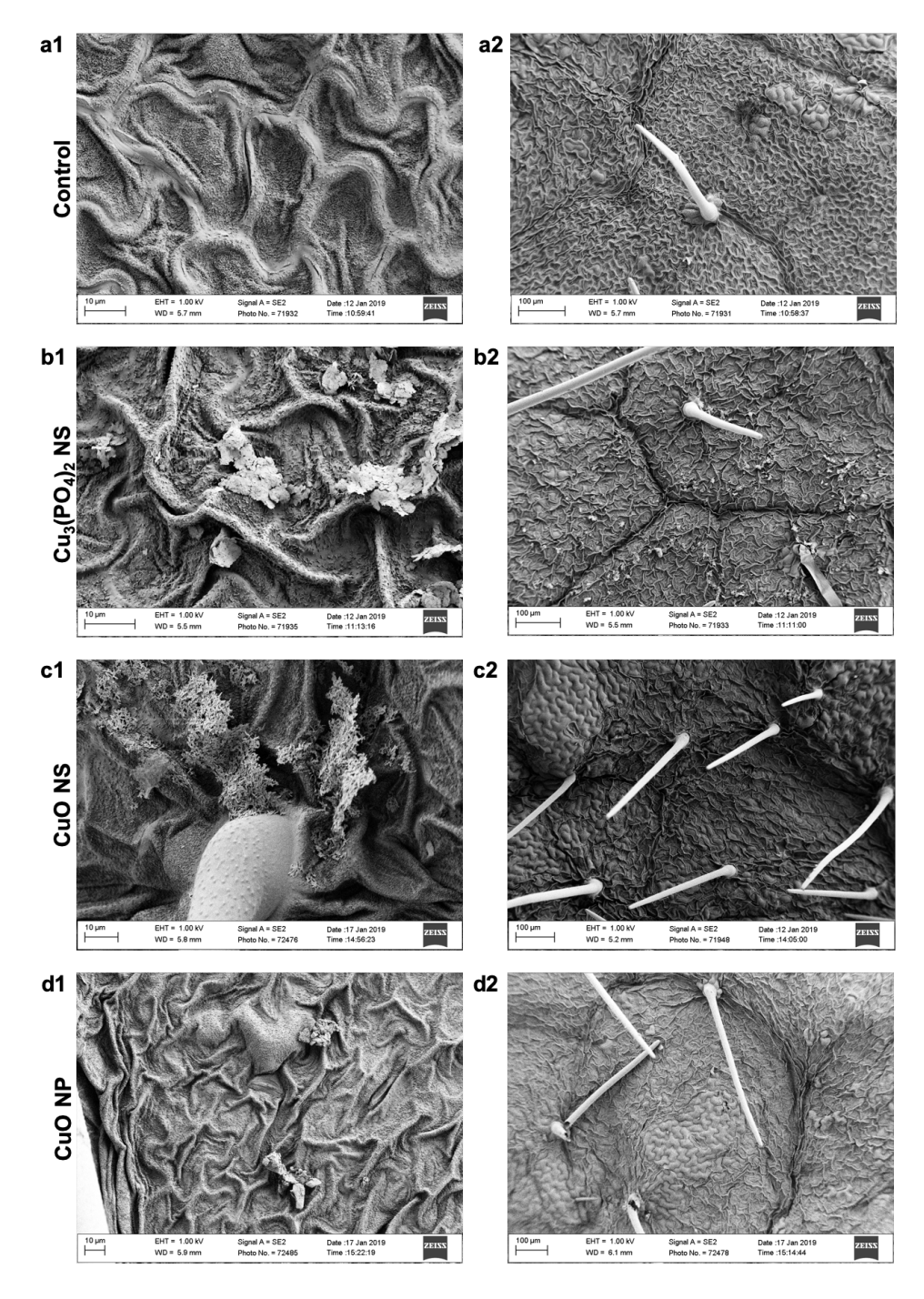


Figure 4. Cu-based NM distribution in FV infected soybean foliar treated with 250 mg/L NM suspensions three times with one-week interval. Figure **a1-d1** represents Cu-based NM distribution on the soybean leaf surface in the control, $Cu_3(PO_4)_2$ NS, CuO NS, and CuO NP treatment, respectively. Figure **a2-d2** represents the pattern of Cu-based NM distribution in the area of trichomes in the control, $Cu_3(PO_4)_2$ NS, CuO NS, and CuO NP treatment, respectively.

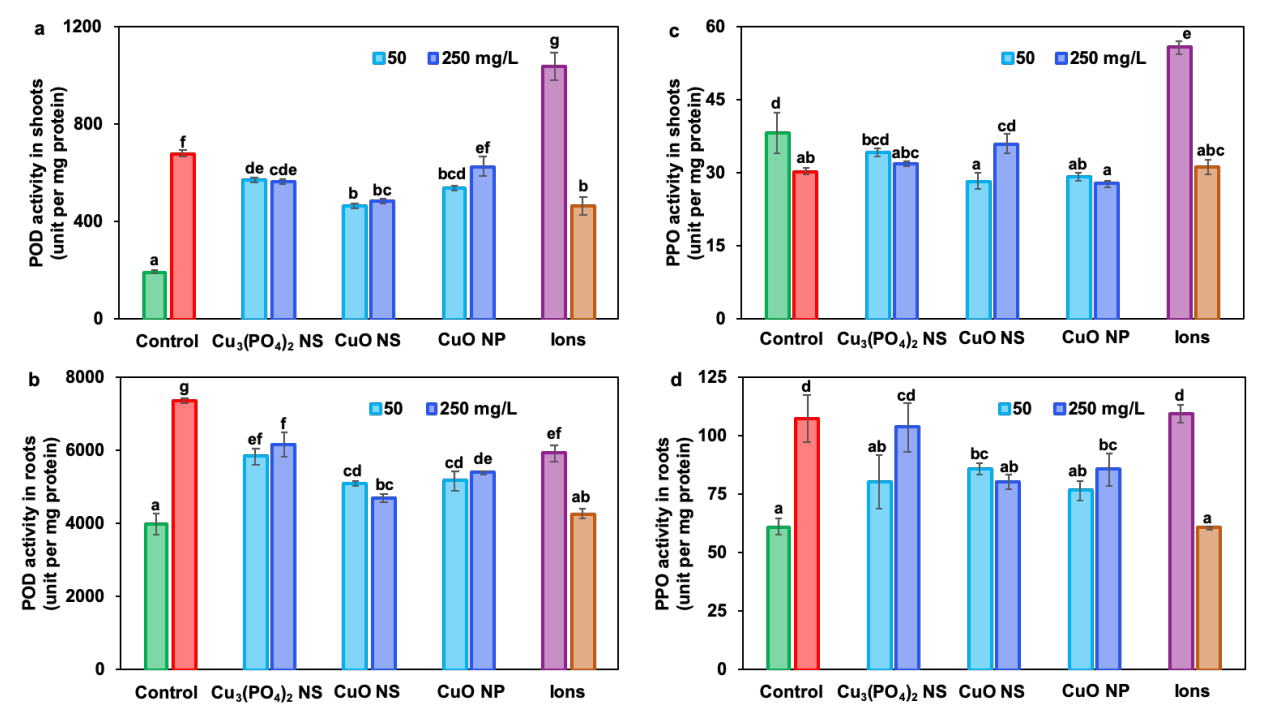


Figure 5. POD and PPO activity in FV infected soybean upon foliar-exposure to different types of Cu-based NMs. Figure **a-b** shows the POD activity in shoots and roots, respectively, in the FV treatments with different types of Cu-based NMs at 50 and 250 mg/L (mass of particles); Figure **c-d** represents the PPO activity in shoots and roots, respectively, in the FV treatments with different types of Cu-based NMs at 50 and 250 mg/L (mass of particles). In each panel, green bar (□) and red bar (□) represents healthy control and diseased control, respectively; blue bars represent the treatments with different types of Cu-based NMs at 50 and 250 mg particles/L; purple bar (□) and brown bar (□) represents 1.725 mM [Cu] ionic control and 1.175 mM [PO₄³⁻] ionic control, which is the same molar concentration of [Cu] and [PO₄³⁻] in 250 mg/L Cu₃(PO₄)₂ NS, respectively. Error bars correspond to standard error of mean (n=4); values followed by different letters are significantly different at p<0.05.

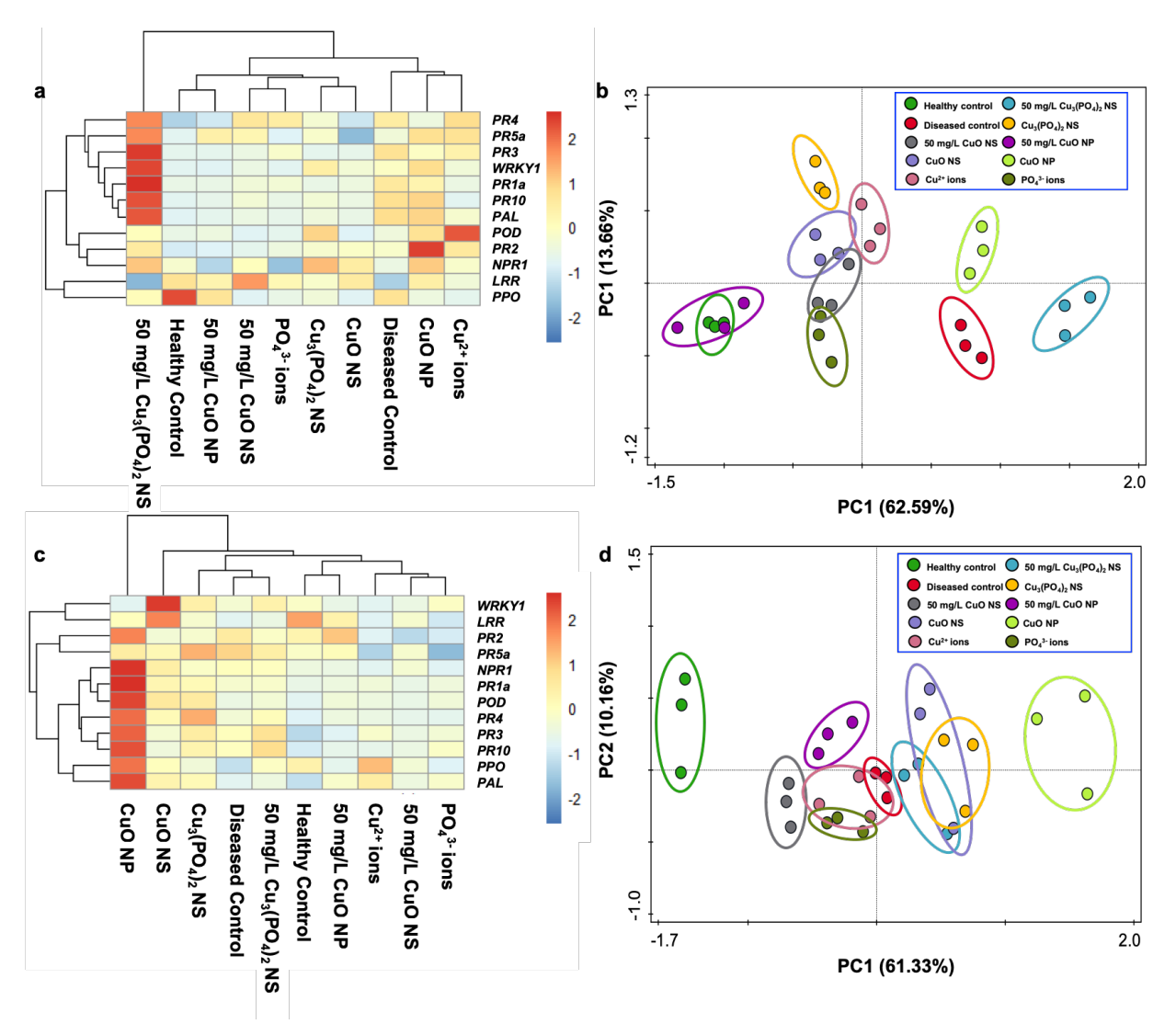


Figure 6. Heatmap and PCA analysis of the relative expression of disease-related genes in FV infected shoots (**a**, **b**) and roots (**c**, **d**) as affected by different types of Cu-based NMs at 50 mg/L (mass of particles) or the equivalent amount of Cu (1.725 mM). Disease-related genes reported above include pathogenesis-related genes (PR1a, PR2, PR3, PR4, PR5a, PR10), NPR1 protein, WRKY1 transcription factor, leucine-rich repeat (LRR), antioxidant enzymes (POD, PPO and PAL). Gene fold-change was expressed relative to the FV control plants. CuSO₄ and Na₃PO₄ with 1.725 mM Cu²⁺ and 1.15 mM PO₄³⁻, respectively, was used as the Cu²⁺ and PO₄³⁻ ionic control.